

Roche Lobe Overflow from Dwarf Stellar Systems.

Stephen D. Murray

University of California, Lawrence Livermore National Laboratory, P.O. Box 808, Livermore, CA 94550

Shawfeng Dong, & Douglas N. C. Lin

University of California, Lick Observatory, Santa Cruz, CA 95064

ABSTRACT

We examine the evolution of residual gas within tidally-limited dwarf galaxies and globular clusters. In systems where the gas sound speed exceeds about 10% of the central velocity dispersion, hydrostatic equilibrium causes the gas to have significant density at the tidal radius. In contrast to the stellar component, gas particles relax rapidly in response to mass loss. Gas lost through the Lagrangian points is quickly replenished, leading to continuous outflow, analogous to the Jeans' escape of planetary atmospheres. In such systems, the gas may be lost on timescales as short as a few times the sound crossing time of the system. In colder systems, by contrast, the density contrast between the core and the tidal radius is much larger, greatly reducing the mass loss rate, and allowing the system to retain its gas for over a Hubble time. Using this criterion as a guide, we present the results of numerical simulations to show that either in the proximity of large galaxies or in clusters of galaxies, residual gas in typical dwarf spheroidal galaxies (dSphs) and globular clusters would be efficiently lost after it is ionized and heated, either by external or internal sources. The tidally removed gas shall follow an orbit close to that of the original host system, forming an extended stream of ionized, gaseous debris. Such tidal mass loss severely limits the ability of dSphs and globular clusters to continuously form stars. The ordinary gas content in many dwarf galaxies is fully ionized during high red-shift epochs. In extreme cases, therefore, star formation may be completely prevented by early segregation of dark and ordinary matter, leading to the formation of starless, dark-matter concentrations as the remnants of dwarf galaxy mergers in the CDM model of galaxy formation. In the field, where the dwarf galaxies are tidally isolated, and in the center of clusters of galaxies, where the tidal potential is compressive, ionized gas may be retained by dwarf galaxies, even though its sound speed may be comparable to or even exceed the velocity dispersion. In such situations, dwarf galaxies may retain their gas content until they merge with much larger galaxies. These processes may help to explain some observed differences among dwarf galaxy types, as well as observations of the haloes of massive galaxies.

Subject headings: galaxies: dwarf — galaxies: evolution — clusters: globular — clusters: open — hydrodynamics — methods: numerical

1. Introduction

In the widely adopted cold dark matter (CDM) cosmological models, small objects are the first to form, and larger galaxies form via the merger of dwarf systems (e.g. White & Rees 1978; Blumenthal et al. 1984; Cole et al. 1994; Klypin, Nolthenius, & Primack 1997; Navarro, Frenk & White 1997). The evolution

of the smaller building blocks is therefore of great interest for the evolution of larger systems. Because they formed prior to the emergence of normal galaxies, these subsystems are theoretically expected to have greater density than the larger systems, and therefore they are likely to retain their integrity in the halo of large host galaxies, which would imply the existence of many more surviving systems than are observed today (Moore et al. 1999). The lack of small stellar systems around larger host galaxies has been referred to as the “missing satellite” problem (Klypin et al. 1999).

One possible resolution of the problem is that gaseous baryonic matter may have been ejected from the dwarf systems due to massive star formation, which in turn leads to photoionization-driven outflows, stellar winds, and supernovae (Tenorio-Tagle et al. 1986; Efstathiou 1992; Lin & Murray 1994; Quinn, Katz, & Efstathiou 1996; Kepner, Babul, & Spergel 1997; Navarro & Steinmetz 1997; Weinberg, Hernquist & Katz 1997; Barkana & Loeb 1999; Benson et al. 2002; Dong, Murray, & Lin 2003; Dekel & Silk 1986; Mac Low & McCray 1988; Madau, Ferrara, & Rees 2001; Mori, Ferrara, & Madau 2002). Once segregated, the ordinary matter continues to its dissipational infall, while the dark matter components form a lumpy halo in the potential of the large galaxy (Weil, Eke & Efstathiou 1998; Sommer-Larsen, Gelato, & Vedel 1999). If the mass loss is driven by bursts of star formation, a small amount of residual ordinary matter, which has already been converted into stars, would remain with the clumpy dark matter subsystems.

In the halo of the Galaxy, several dwarf spheroidal galaxies (dSphs) are found in the form of diffuse patches of stellar light (Hodge 1971) embedded in dark matter haloes (Aaronson 1983; Faber & Lin 1983). It is natural to identify these with the remnant subsystems, *i.e.* the theoretical building blocks of large host galaxies in the CDM scenario (Mateo 1996; Klypin et al. 1999; Moore et al. 1999), because they have similar total mass ($\gtrsim 10^{7-8} M_{\odot}$). There are, however, significant differences. Both the small (few km s^{-1}) velocity dispersions, and the inferred dynamical density of the observed dwarf galaxies are smaller than those postulated in the CDM models. Also, the spread in the observed amount of luminous matter (and hence the mass to light ratio) in the dSphs is much larger than that in their total mass (Mateo 1998).

Some of the above differences may be due to evolution. The dSphs are found to have a wide range of star-formation and enrichment histories, with few clear trends (Mateo 1998; Grebel 2001; Harbeck et al. 2001). All contain populations of old stars of varying sizes, and ages exceeding 10 Gyr. In addition, some show histories of continuous star formation, many others show evidence of bursts of star formation separated widely in time, and a few show little or no evidence of subsequent star formation. The observed stellar population and the modest mass-to-light ratio of the dSphs are consistent with the hypothesis that a significant fraction of the original baryonic matter may have been ejected from them and other dwarf galaxies as a consequence of earlier epochs of star formation (Gerola, Carnevali, & Salpeter 1983; van Zee, Skillman, & Salzer 1998).

In addition to dSphs, the families of low-mass, gas-poor dwarf stellar systems also include dwarf elliptical galaxies, and globular clusters. These groups of objects are quite distinct from each other (Kormendy 1985). Some of their differences may, however, result from post-formation evolution processes, such as mass loss either prior to or following star formation (see discussion above), or segregation of baryonic and dark matter during star formation (Murray & Lin 1989). The globular clusters are the low-mass extreme of these families of dwarf stellar systems. Their velocity dispersions are generally more than twice that of the dSphs within the Local Group of galaxies, but less than that of typical dwarf elliptical galaxies within nearby clusters of galaxies. In contrast to the dwarf spheroidal galaxies, all but one or two globular clusters of the Milky Way show evidence for only a single, old stellar population. As in those dwarf galaxies which show little evidence for more than a single generation of star formation, any gas within globular clusters that remained after the initial generation of stars formed must have been lost from within them. Nevertheless, the multiple

populations of stars in at least one globular cluster (ω Cen) and several dwarf galaxies indicate that the star formation process may not always be an effective mechanism for decoupling the ordinary and dark matter in these loosely bound stellar systems.

Collectively, the population of the observed dwarf stellar systems falls far below that predicted in the CDM model, and so they alone cannot be the resolution of the “missing satellite” problem. Gravitational lensing observations, however, find preliminary indications of starless dark matter clumps in the halos of nearby galaxies (Metcalf 2002; Metcalf & Zhao 2002). If such dark entities dominate the halo structure, then an efficient and severe segregation of ordinary and dark matter, through processes in addition to the violent impact of star formation, is needed. A more quiescent process may therefore also play a significant role in determining the ability of dwarf stellar systems to retain their gas to form multiple generations of stars (Lin & Murray 1998). We shall address the cause of multiple generations of stars in dwarf spheroidal galaxies in a separate paper.

Several gas dynamical processes may lead to gas removal from stellar systems with shallow potentials. Prior to star formation, gas may be removed by either ram-pressure or Kelvin-Helmholtz instability resulting from motion through the halo gas of a larger system (Lin & Faber 1983; Murray et al. 1993). The efficiency of gas removal due to either process depends upon the depth of the gravitational potential, and the density of ambient gas. While it is possible that the dwarf galaxies and globular clusters seen today were able to retain sufficient gas to form stars within them because they have deeper potentials than the dark matter-dominated “missing satellites,” the amount of ambient gas in the halo of the large, host galaxies is highly uncertain.

In the halo of the Milky Way and other galaxies, both satellite dwarf galaxies and star clusters are subject to tidal forces. For dSphs, this process occurs following the formation of a nearby, massive galaxy, whereas star clusters form within the potential of a massive system. The tidal forces increase rapidly in significance for smaller orbits around the host galaxy, and can strongly perturb any ionized gas within the satellite stellar systems. The resulting situation is somewhat analogous to that of interacting binary stars (Pringle 1985), in that the ionized gas in the satellite systems always relaxes, and expands to fill their Roche Lobes. A fraction of the gas continually streams away from the satellite systems through their inner and outer Lagrange points. If the rate of gas loss is substantial, it may limit the ability of dwarf systems to retain gas for subsequent generations of star formation.

In this work, we examine the significance of mass loss from tidally-limited dwarf systems. We begin in Section 2 with an analytic estimate of the rate of mass loss. In Section 3, we examine the results of simple one-dimensional models, and continue with three-dimensional models in Section 4. Our results are summarized and consequences for the evolution of dwarf systems are drawn in Section 5.

2. Analytic Determination of Mass Loss Rates

The distance of the L1 and L2 points from the center of the dwarf satellite are given approximately by the Roche radius,

$$R_R = a \left(\frac{M_d}{M_d + M_G} \right)^{\frac{1}{3}} \left[\frac{1 - e}{(3 + e)^{\frac{1}{3}}} \right], \quad (2-1)$$

for a point-mass parent-galaxy potential (King 1962), and

$$R_R = a \left(\frac{M_d}{M_d + M_G} \right)^{\frac{1}{3}} \left\{ \frac{(1 - e)^2}{[(1 + e)^2/2e] \ln[(1 + e)/(1 - e)] + 1} \right\}^{\frac{1}{3}}, \quad (2-2)$$

for a logarithmic parent-galaxy potential (Oh & Lin 1992). In the above expression, M_d is the total mass (gas, stars, and dark matter) of the satellite system. The parent galaxy has mass M_G inside the orbital semimajor axis a of the satellite system. Although the concept of the tidal radius for a satellite with an orbital eccentricity e is uncertain and controversial (Innanen 1979; Allen & Richstone 1988), it provides a useful fiducial length scale (Oh & Lin 1992). The above results may be parameterized as

$$R_R = a \left(\frac{1}{\beta} \frac{M_d}{M_d + M_G} \right)^{\frac{1}{3}} \quad (2-3)$$

where β is a function of e . For circular orbits around a point mass potential, $\beta = 3$, whereas around an isothermal potential, $\beta = 2$.

The rate of mass loss through the Lagrange points is related to the Roche radius and the sound speed of the gas, c_s . A full derivation in the context of a low-mass planet orbiting around a main sequence star is given in Gu, Lin & Bodenheimer (2002). For the total loss rate of gas through the L1 and L2 points, the results can be approximated as

$$\dot{M}_g = 4\pi\rho_1 R_R^2 c_s f, \quad (2-4)$$

where ρ_1 is the gas density at the Roche radius. The geometrical correction factor, f , can be approximated by expanding the potential near the Lagrangian point (see 4-3).

If the gas within the dwarf system is isothermal, and the potential of the system is approximated with a Plummer potential (Binney & Tremaine 1987), then the gas density varies as

$$\rho_g(r) = \rho_0 \exp \left[\frac{-(\phi(r) - \phi_0)}{c_s^2} \right], \quad (2-5)$$

while

$$\phi(r) = \frac{-GM_d}{(R_c^2 + r^2)^{1/2}}, \quad (2-6)$$

where $\phi_0 = \phi(r=0) = -GM_d/R_c$. In the above, R_c is the core radius, defining the radius over which the density of gravitating matter is approximately constant. In this potential, the ratio of the gas density at R_R to that at the center (ρ_0) is

$$\frac{\rho(R_R)}{\rho_0} = \exp \left[\frac{\alpha}{(1 + x_R^2)^{1/2}} - \alpha \right] \quad (2-7)$$

where $x_R = R_R/R_c$, and

$$\alpha \equiv \frac{GM_d}{R_c c_s^2}. \quad (2-8)$$

Even for relatively concentrated systems where $x_R \gg 1$, the gas density retains a finite value at large radius, albeit $\rho(R_R)/\rho_0$ can be very small for cold gas, with large values of α . For large values of $\rho(R_R)$, self-gravity of the gaseous envelope may become important, and the gas shall become a self-gravitating isothermal sphere, resulting in a more rapid decline in density than assumed here.

In response to mass loss, the gas adjusts on a sound crossing time in an attempt to re-establish a density distribution appropriate to hydrostatic equilibrium. Any loss from the system at large radii is therefore continually replenished. This is in contrast to the stars, which diffuse on the much-longer two-body relaxation time scale. Thus, the mass loss rate of the gas, \dot{M}_g remains approximately constant prior to any significant reduction in \dot{M}_g .

The total mass of isothermal gas within the dwarf system is given by

$$M_g = 4\pi \int_0^{R_R} \rho_g(r) r^2 dr = 4\pi \rho_c R_c^3 \int_0^{x_R} \exp\left[\frac{-(\phi(r) - \phi_0)}{c_s^2}\right] dx \quad (2-9)$$

where $x = r/R_c$. For a Plummer potential,

$$M_g = 4\pi \rho_0 R_c^3 \int_0^{x_R} \exp\left\{\alpha \left[\frac{1}{(1+x^2)^{1/2}} - 1\right]\right\} x^2 dx. \quad (2-10)$$

Note that, for sufficiently large x_R , the dwarf galaxy's potential can contain an arbitrarily large mass, even in the hot limit where $\alpha < 1$. But for modest values of either x_R or R_R , the mass of gas within the potential is limited.

Using Equations (2-2), (2-4), and (2-10), and assuming the dwarf satellite to be on a circular orbit of period

$$P = 2\pi \left(\frac{a^3}{GM_G}\right)^{\frac{1}{2}}, \quad (2-11)$$

the mass loss time scale becomes

$$\tau_{loss} \equiv \frac{M_g}{\dot{M}_g} = \frac{\Gamma(x_R, \alpha) P}{f}, \quad (2-12)$$

where

$$\Gamma(x_R, \alpha) \equiv \exp\left\{\alpha \left[1 - \frac{1}{(1+x_R^2)^{\frac{1}{2}}}\right]\right\} \frac{1}{x_R^3} \left(\frac{\alpha}{x_R \beta}\right)^{\frac{1}{2}} \frac{1}{2\pi} \int_0^{x_R} \exp\left\{\alpha \left[\frac{1}{(1+x^2)^{\frac{1}{2}}} - 1\right]\right\} x^2 dx \quad (2-13)$$

gives the number of orbits of the dwarf satellite around the parent system before significant mass loss occurs.

In the limit of cold gas, $\alpha \gg 1$ and

$$\tau_{loss} \simeq \left(\frac{R_c c_s^2}{GM_d}\right) \exp\left\{\frac{GM_d}{R_c c_s^2} \left[1 - \frac{1}{(1+x_R^2)^{1/2}}\right]\right\} \frac{P}{(2\pi\beta)^{1/2} x_R^{7/2} f} \gg P \quad (2-14)$$

so that over a Hubble time scale, no significant mass loss occurs. But, for $\alpha < \alpha_1$, where

$$\frac{1}{\alpha_1} \exp\left[\alpha_1 - \frac{\alpha_1}{(1+x_R^2)^{1/2}}\right] \simeq (2\pi\beta)^{1/2} x_R^{7/2} f, \quad (2-15)$$

a significant amount of gas is lost within an orbital period.

In Figure 1, we show the variation of $\Gamma(x_R, \alpha)$ with α (panel A) and with α' (panel B) for three values of x_R , selected to match the values used in the one- and three-dimensional dwarf galaxy models discussed in the next two sections. For these calculations, we choose $\beta = 2$, corresponding to a circular orbit in an isothermal host-galaxy potential. The quantity α' is defined as

$$\alpha' \equiv \alpha \left[1 - (1+x_R^2)^{-\frac{1}{2}}\right], \quad (2-16)$$

such that $\alpha'^{1/2}$ corresponds to the Mach number of the escape speed from the center to the Roche radius.

As can be seen from panel A of Figure 1, and as would be expected from Equations 2-12 and 2-13, the time scale for loss of gas may become extremely short, less than the orbital period, if $\alpha < \alpha_1 \sim 10 - 15$. The

curves of $\Gamma(x_R, \alpha)$ vs. α for $x_R = 1, 3$, and 9 cross each other for large α . We note, however, from panel B of Figure 1, that for $\alpha > 1$, $\Gamma(x_R, \alpha)$ is a more sensitive function of α' than of α . The critical condition for rapid mass loss, $\Gamma(x_R, \alpha) = 1$, occurs when $\alpha' = \alpha'_1 \simeq 5 - 10$, depending on the value of x_R .

The observed velocity dispersions of dwarf stellar systems, which are indicative of the potential depths, are similar to the sound speed of ionized gas (Mateo 1998; Pryor & Meylan 1993). Once the gas in these systems is ionized, either by internal or external sources, it shall have $\alpha' \sim 1$. In this limit, the results in Figure 1B imply that the ionized gas may be rapidly lost by a continuous, quiescent outflow, thus preventing the formation of subsequent generations of stars. Subsequent stellar generations would form only if gas could be accreted, a possibility which shall be examined in a subsequent paper.

3. One-Dimensional Models

In the analytic model presented above, the gas is assumed to be in quasi-hydrostatic equilibrium at all times. Yet, mass loss leads to outflow and a reduction in the residual gas mass which should be treated with a time-dependent dynamical calculation. We examine the time evolution of the gas in dwarf galaxies and star clusters using numerical simulations. In order to compare with the analytic results above, we first carry out a series of one-dimensional dynamical simulations. Using these models, we show the importance of ionization and gas temperature on the rate of tidally induced outflow.

The one-dimensional scheme used was first developed to study star formation and feedback effects in dwarf galaxies (Dong, Murray, & Lin 2003). It is a 1D Lagrangian code, into which radiative transfer and photoionization are incorporated using a Strömgren shell model. It thus allows us to explore the effects of heating and photoionization by both internal and external UV sources. With a Lagrangian scheme, we also do not need to specify artificial conditions near the boundaries of the computational domain. Gas is allowed to freely flow out of the region.

For the 1D models, the gas experiences the gravity of the dark matter of the dwarf galaxy, as well as an external tidal potential. The dark matter potential of the dwarf galaxy is taken to follow the form found by Burkert (1995), which has been tested to be a slightly better fit to dwarf spheroidal galaxies than the simpler Plummer potential, used in the previous section. The corresponding dark matter density distribution is given by

$$\rho_{DM} = \frac{\rho_c r_0^3}{(r + r_0)(r^2 + r_0^2)}. \quad (3-1)$$

The central density and velocity dispersion of the dwarf galaxies are scaled with a structural length scale r_0 such that

$$\rho_c = 4.5 \times 10^{-2} (r_0/\text{kpc})^{-2/3} M_\odot \text{pc}^{-3}, \quad (3-2)$$

$$\sigma = 17.7 (r_0/\text{kpc})^{2/3} \text{km s}^{-1}, \quad (3-3)$$

The gravitational potential due to the dark matter within the dwarf galaxy is determined from its density using Poisson's equation. From equations (2-5) and (2-10), we can determine the density distribution of an isothermal gas in this potential, including its central value ρ_0 . In order to determine the extent of the dwarf galaxy, we also impose an external tidal potential, chosen to follow the form

$$\phi_{tide} = \phi_0 \left[1 + \left(\frac{r}{r_0} \right)^\lambda \right] \quad (3-4)$$

where $\phi_0 < 0$. The exact value of λ is found to be unimportant; in the following calculations, we choose $\lambda = 1$. We specify the tidal radius R_R to be the location where the gradient of the total potential vanishes. One can show that R_R/r_0 is related to ρ_c and ϕ_0 as

$$\phi_0 = -\frac{2\pi G\rho_c r_0^4}{\lambda R_R^2} \left(\frac{R_R}{r_0}\right) \left\{ \ln\left(1 + \frac{R_R}{r_0}\right) + \frac{1}{2} \ln\left[1 + \left(\frac{R_R}{r_0}\right)^2\right] - \arctan\left(\frac{R_R}{r_0}\right) \right\} \quad (3-5)$$

The initial distribution of gas is set up in hydrodynamic equilibrium under the dark matter potential alone. The total mass of gas, $M_g = qM_{DM}$, where the ratio of baryonic to dark matter q is assumed to be 0.1 in most of our calculations (Mateo 1998). At the onset of the calculations, both the external potential and extragalactic UV radiation are switched on instantly. The residual gas quickly settles into a quasi-equilibrium after a brief and minor adjustment in the outermost region. Because the gas density is tenuous in this region, this adjustment does not affect the subsequent evolution of the gas.

We assume the gas to be metal-free, so that in the absence of photoionization it would cool to a temperature $T \sim 10^2 K$ (Kang et al. 1990; Lin & Murray 1992). The temperature of the photoionized gas is taken to be 15,000 K, appropriate for low-metallicity, photoionized gas. The external UV flux $J_\nu \approx 10^{-23}$ ergs s⁻¹ cm⁻² ster⁻¹ Hz⁻¹ at the Lyman limit at low redshift, and 50 times more intense at redshift $z = 3$ (cf. Haardt & Madau 1996), is sufficient to completely ionize most dSphs, as confirmed by our models. More massive dwarf elliptical galaxies (dEs), are, however, partially self-shielded from the external UV, and so they contain a region of neutral residual gas surrounded by ionized gas. Because we are, in this section, primarily interested in the efficiency of photoionization for dEs, the model parameters used here are appropriate to those systems. In the next section, we present the results of some 3-D models for the evolution of fully ionized gas within dSphs.

The properties of the one-dimensional models are shown in Table 1. For each model, we list M_d , r_0 , the escape speed from the central potential (σ , equivalent to GM_d/R_c in the previous section), α' for the ionized gas, J_ν , the initial baryonic mass fraction (M_{gi}/M_d), the ratio of the final mass of neutral gas to the initial total gas mass (M_{Hf}/M_{gi}), the ratio of the initial radius of the sphere of neutral gas to the Roche radius (R_R/R_n), P , the computed mass loss timescale for gas (τ_{loss}), the ratio of τ_{loss} to P , and the computed value of Γ .

In the standard model (1D-1), $r_0 = 1$ kpc, such that $\sigma \simeq 18$ km s⁻¹. In this and all other models presented here, we set $R_R = 3r_0$, so that the dwarf galaxy's total mass $M_d \simeq 5M_0$ where M_0 is the total mass within r_0 . In Model 1D-1, the galaxy's mass (including both dark and gas components) within r_0 and R_R are, respectively, $M_0 = 7.2 \times 10^7 M_\odot$ and $M_d = 3.66 \times 10^8 M_\odot$.

If the dwarf galaxy has a circular orbit in an isothermal potential of the background host galaxy, with circular speed $V_c = 210$ km s⁻¹, and mass

$$M_G = 5 \times 10^{11} (a/50\text{kpc}) M_\odot, \quad (3-6)$$

the orbital radius a is given by Equation (2-3). The orbital period, $P = 1.49 (a/50 \text{ kpc})$ Gy and $\beta = 2$. For Models 1D-1, 1D-2, 1D-3, and 1D-4, we adopt $r_0 = 1$ kpc so that $a = 129.1$ kpc and $P = 3.85$ Gy. For Model 1D-5, we choose $r_0 = 1.35$ kpc, such that $a = 182.6$ kpc and $P = 5.14$ Gyr.

The evolution of the mass fractions of gas within the tidal radius for the one-dimensional models are shown in Figures 2 and 3. As can be seen in Figure 2, half of the gas mass is lost from Model 1D-1 within 350 Myr, in spite of the fact that $c_s \simeq 0.6\sigma$. This result is consistent with our discussion in the previous

section where we showed that a significant fraction of the ionized gas is lost within one galactic orbital period for $\alpha = (\sigma/c_s)^2 < \alpha_1 \simeq 10$. Such rapid outflow of gas would prevent extended and protracted star formation. The ionized gas at the outskirts of the galaxy flows beyond R_R with the sound speed ($\sim 10 \text{ km s}^{-1}$) of the ionized gas.

In Model 1D-1, $J_\nu = 4 \times 10^{-23} \text{ ergs s}^{-1} \text{ cm}^{-2} \text{ ster}^{-1} \text{ Hz}^{-1}$, appropriate for redshift $z = 1$. In this model, a small amount, M_{Hf} , of the residual gas remains in a neutral state at the center of the galaxy, surrounded by ionized gas at an interface of radius R_n . In Figure 4 are shown snapshots of the densities of the neutral and ionized gas, ρ_n and ρ_i for the first four one-dimensional models, as a function of radius. These results show that, analogously to the Strömgren sphere in an HII region, the ionization front contracts slowly from the outer tenuous to the inner, denser regions of the galaxy, while the ionized gas lost from the outer halo is being continually replenished.

When a quasi-static equilibrium is established, in which the external UV flux is balanced by recombination in the outer ionized envelope, the magnitude of $\rho_i \propto J_\nu^{1/2}$ (Figure 4), while c_s is independent of J_ν . We thus expect $\dot{M} \propto J_\nu^{1/2}$. This conjecture is confirmed by Models 1D-2 and 1D-3 which have identical structural parameters as Model 1D-1, but reduced J_ν . In these cases, both the mass fraction and radius of the neutral sphere are larger than the standard model. Similar to the standard model, $\alpha \simeq 1 < \alpha_1$ in the ionized envelope and the ionized gas flows from the ionization front at R_n to R_R in a fraction of the sound crossing time. The density of ionized gas at R_R is, however, reduced relative to the standard model, due to the larger masses of cold, neutral gas, with its steeper radial density falloff. The result is a reduction in \dot{M}_d relative to the standard model. The actual dependence of J_ν upon redshift remains uncertain, and the values listed in Table 1 are comparable to the values estimated for the present epoch by some authors (Haardt & Madau 1996; Bechtold et al. 1987; Ostriker & Ikeuchi 1983).

In Model 1D-4, we increase the ratio, q , of the baryonic-to-dark matter mass by a factor of two from the standard model. The increased density of baryonic matter enhances self-shielding, and the gas becomes mostly neutral. The gas cools and settles to the center of the galaxy, with a smaller R_n . The ionization rate across the front is balanced by rapid recombination, making photo-evaporation less efficient. Consequently, the value of ρ_i decreases, and the mass loss rate is reduced (Figure 3). In Model 1D-5, we increase r_0 by a factor of 1.35 but maintain the baryonic fraction at 0.1. In accordance with the Burkert (1995) potential, \dot{M}_d in Model 1D-5 is twice that in Model 1D-1, though the initial gas mass M_{gi} is the same as Model 1D-4. With these parameters, gas in the center of the dwarf galaxy is less dense, but the total baryonic mass is greater than in the standard model. Once again, the larger gas reservoir enables a greater fraction of M_{gi} to become self-shielded, neutral, cool, and settle to the center of the galaxy, again reducing the mass loss rate relative to the standard model.

We have also computed a case which has identical physical parameters as Model 1D-1, but the galaxy is set in isolation (infinite tidal radius). In this case, the gas adjusts to both ionization and hydrostatic equilibrium with no gas attaining finite outflow velocity. As indicated above, even for the early epochs where z and J_ν are large and the gas is fully ionized and hot, these static equilibria can be attained from Equations (2-5) and (2-10) with a sufficiently large x_R or equivalently R_R . The implications of these results will be discussed in § 5.

4. Three-Dimensional Models

The one-dimensional models provide the basic description for the underlying ionization, relaxation, and hydrodynamics of the residual gas which regulate the efficiency of its tidally induced outflow. But in reality, the tidal forcing of the host galaxy is non-spherically symmetric about the center of the dwarf galaxy. In order to consider a more realistic tidal potential, we examine the results of some three-dimensional simulations in this section.

4.1. Numerical Method

The numerical code we use is Cosmos. It is a massively parallel, multidimensional, radiation-chemo-hydrodynamics code developed at Lawrence Livermore National Laboratory. The code, and tests of the code are described in Anninos & Fragile (2003), and Anninos, Fragile & Murray (2003). It has also been used to study the evolution of supernova-enriched material in dwarf galaxies by Fragile et al. (2003). The reader is referred to those papers for more details on Cosmos. We discuss here the settings used for the current work.

We wish to examine the evolution of either cool or heated gas within dwarf galaxies and massive star clusters. The one-dimensional models discussed above include the effects of heating, cooling, and ionization of the gas and show that the gas dynamics is primarily determined by its temperature and more indirectly by the state of ionization. For the three-dimensional models, the inclusion of ionization and recombination of the gas would only reduce the controlled nature of the models, without adding new information. Thus, we choose to set the gas to be initially isothermal, at a determined temperature. In order to approximate the effects of heating and cooling, which has the tendency to maintain the gas at a nearly constant temperature, we assume that the gas evolves adiabatically, with exponent $\gamma = 1.1$. We choose two sets of models. For the hot models, we set the gas temperature to be 8,000 K and for the cold model we assume the gas is in an atomic state with a temperature of 1,000 K. These isothermal states correspond to either early or recent epochs, when J_ν is either adequate or insufficient to significantly ionize the residual gas. The results of the 1-D models in the previous section indicate that, for dSphs, the entire galaxy is likely to be ionized by a modest external UV flux. Thus an isothermal temperature is a reasonable approximation for the hot models. When the gas attains a sufficiently large density, it becomes self-shielded inside these galaxies and clusters. The isothermal approximation is also sufficient for this cool phase.

Self-gravity of the gas is not included in the models. This approximation should be adequate for dwarf galaxies, which are dark-matter rich, and so their gravity is dominated by that of the dark matter. For a globular cluster, which has undergone efficient star formation, the potential is dominated by the stars, and so, again, the potential of the gas is not important to the evolution. The models therefore include a static background potential, within which the gas evolves. In order to compare the numerical results with our analytic calculations, the background is modeled as a Plummer potential, as expressed in Equation (2-6), which has a form similar to, but simpler than, those found to be followed by dwarf galaxies (Berkert 1995), and which has also been used to model globular clusters (Plummer 1911).

To the potential of the dwarf stellar system is added that of a massive parent galaxy. The total density of the massive parent galaxy is assumed to follow the same isothermal form as above, with a total mass of $5 \times 10^{11} M_\odot$ and a circular speed $V_c = 210 \text{ km s}^{-1}$ at some typical distance 50 kpc from the Galactic center. Smaller Galactic radii are used for the globular cluster models.

Throughout the numerical simulations, our models remain centered upon the dwarf systems, ie. we are

in a non-inertial frame of reference. Coriolis terms must therefore be added to the potential, which then has the form

$$\phi(x, y, z) = \phi_d(x, y, z) + \phi_G(x, y, z) - \frac{1}{2}\Omega^2 (x^2 + y^2), \quad (4-1)$$

where $\phi_{d,G}$ are the conservative gravitational potentials of, respectively, the dwarf stellar system and parent galaxy, Ω is the angular velocity of the rotating frame (the system is assumed to be in a circular orbit), the z -axis is the axis of rotation, and the x -axis points towards the center of the parent galaxy. This form of the effective potential is analogous to that used for close binary stars (Pringle 1985).

The form of the potential is shown in Figure 5, which shows a surface plot of $\phi(x, y, 0)$ for Model 3D-1d. Positions on the x and y axes, and the potential are all in code units. The L1 and L2 points are located along the x -axis, at $x = \pm x_t$, where $x_t = 0.89$ in code units. Due to the saddle-shape of the potential at L1 and L2, mass loss may occur only near the Lagrange points. At an orbital radius a where $M_d \ll V_c^2 a/G$

$$x_t = \pm \left[\left(\frac{GM_d}{2\Omega^2 R_c^3} \right)^{2/3} - 1 \right]^{1/2} R_c \quad (4-2)$$

which reduces to $x_t \simeq (GM_d/2\Omega^2)^{1/3}$ in the limit that $R_c \ll (GM_d/2\Omega^2)^{1/3}$. In comparison with our analytic, spherically symmetric approximation, x_t is the analogous quantity to R_R , and is only slightly modified from the expression for the Roche radius of a point-mass potential for the dwarf galaxy.

In the vicinity of x_t , the gas density is approximately constant because the gradient of ϕ vanishes, such that the density scale height of the gas diverges at x_t . The escaping gas streams out of the dwarf galaxy through the saddle surfaces, which are bounded by the local potential maxima in which $\partial\phi/\partial x = 0$. This surface lies approximately on the $y - z$ plane, centered on $x = x_t$. For $x_t > GM_d/C_s^2$, we can estimate the magnitude of f (cf. Equation 2-4) under the assumption that gas diffuses to the outflow channels in a hydrostatic manner, such that

$$\begin{aligned} f &\sim \frac{1}{4\pi x_t^2} \int_{-\infty}^{\infty} \int_{-\infty}^{\infty} \exp \left[-\frac{\phi(x_t, y, z) - \phi(x_t, 0, 0)}{c_s^2} \right] dy dz \\ &\sim \frac{x_t c_s^2}{\pi GM_d} \int_0^{\infty} \exp \left(-\frac{3z^2}{4} \right) dz \int_0^{\infty} \left(-\frac{y^2}{2} \right) dz = \left(\frac{2}{3} \right)^{1/2} \left(\frac{x_t c_s^2}{GM_d} \right) \sim \frac{x_R}{\alpha}. \end{aligned} \quad (4-3)$$

Although hydrostatic equilibrium is approximately maintained within the tidal radius, the outflow via the channels prevents the gas from establishing a sustained equilibrium, and that the magnitude of f may be quite different from the above estimate. Nevertheless, the above approximation suggests that f is unlikely to be orders of magnitudes smaller than unity for modest to large values of α' . For $\alpha < 1$, f in Equation (2-4) cannot exceed unity.

In principle, non-inertial terms should also be added to the equations of motion of the gas. These would, however, strongly affect only that gas which was either at or beyond the tidal radius. Because our goal in this work is to examine the rate of mass loss, and not the subsequent evolution of gas lost to the dwarf system, omission of the non-inertial terms shall not affect our conclusions significantly. Our models are generally integrated for a small fraction of an orbit, and so their affect would be small in any event.

The gas density is initially set up such that

$$\rho(x, y, z) = \rho_0 \exp \left[-\phi(x, y, z)/c_s^2 \right], \quad (4-4)$$

where c_s^2 is the isothermal sound speed of the gas. For a spherically-symmetric potential, such an initial distribution of isothermal gas would describe hydrostatic equilibrium. For the non-spherical potential described above, however, the density of the gas near $R = x_t$ evolves significantly at early times. In order to prevent this from causing us to overestimate the mass loss rates, we calculate the mass of gas contained within $R < x_t/2$, which we denote as $M_2(t)$. That quantity shows little affect from the behavior at larger radii. In addition, we avoid influences from early behavior by fitting the value of $M_2(t)$ at late times.

Cosmos is written for Cartesian coordinates, and so we cannot take advantage of the symmetry of the potential to run the problem in two dimensions. In order to reduce computation time, the problems are run as quadrants. Typical resolutions are 200x100x100. We have examined the effects of changing resolutions in some of the models, and find that doubling the resolution changed the time scales for mass loss by only 10%.

4.2. Model Results

The models which we have run in order to examine the evolution of gas within dwarf galaxies are shown in Table 2. On the table are listed, for each model, the total mass of dark matter in the dwarf, M_{dm} , the core radius of the dark matter potential, R_c , the depth of the potential, $\phi_0^{1/2}$ (measured from the center to the galaxy to x_t along the y-axis, i.e. $\phi_0 [1 - (1 + x_R^2)^{-1/2}]$, the orbital radius of the dwarf galaxy around the parent system, a , the value of x_t (i.e. R_R), the initial gas temperature, T_0 , α' , $x_R (= x_t/R_c)$, P , the measured mass loss time scale, τ_{loss} , the ratio $P\Gamma(x_R, \alpha')/\tau_{loss}$, and the equivalent f as derived from Equation (4-3). In the derivation of Γ , we set $\beta = 2$, as in Figure 1. The galaxy parameters are chosen to be representative of small dwarf galaxies (Mateo 1998), and the variations of the parameters examine the effects of mass, orbital radius, and gas temperature upon the mass loss rate. The high temperatures here and below are chosen to be representative of either warm neutral, or warm ionized gas with metal cooling. Throughout the simulation, the gas temperature remains nearly constant.

The values of $M_2(t)/M_2(0)$ are shown in Figure 6. In deriving the values of τ_{loss} quoted in Table 2, the curves have been fitted to the form

$$M(t) = M(0) \exp(-t/\tau_{loss}). \quad (4-5)$$

As can be seen from Figure 6 and below, the curves are not always well represented by exponentials. It is apparent, however, that the derived values of τ_{loss} represent well the rates at which gas is lost from the systems. The time scales for mass loss are comparable to that seen in the one-dimensional case above. In comparison with the analytic results in §2, we find from Equation (2-7) that $f \sim 0.2 - 1.2$ which agrees poorly with that inferred from Equation (2-12). As indicated above, the departure from hydrostatic equilibrium may be the cause of this disagreement. In Figure 7, we plot the mass flow field ($\rho\mathbf{v}$) for Model 3D-4d at 680 Myr. The figure shows a slice in x and y , at $z = 0$. The greatest values of $|\rho\mathbf{v}|$ occur in the complex flow at the center of the galaxy. Away from the center, the vectors of $\rho\mathbf{v}$ are almost parallel to the x -axis. The semi-circle in Figure 7 has radius x_t , and indicates the size of the Roche lobe in the spherical approximation (the actual potential used in the model is highly aspherical, as indicated in Figure 5). Clearly, only a fraction of the Roche surface is open to outflow. The complex flow within the core is time-dependent, but the flow outside of the core is not observed to vary significantly over time. The largest velocities present, near the tidal radius, are 10 km s^{-1} .

Also apparent from the differences of τ_{loss} among the models is the extreme sensitivity to α (cf. Equations 2-12 and 2-13). The critical value of $\alpha' \sim 6$, half the value derived in the analytic approximation. For

$\alpha < \alpha_1$, a significant fraction of the original gas in the dwarf galaxy is lost within an orbital period. The ionized gas in both the lower-mass galaxy and the higher-mass system at lower orbital radius (Models 2 and 4) is largely lost within 1 Gyr, which would preclude extended epochs of star formation.

The globular cluster models are listed in Table 3, which lists the same quantities as in Table 2. The masses and core radii are representative of globular clusters (Pryor & Meylan 1993). The orbital radii are either just outside of the Solar circle, or well within it (most globular cluster orbit closer to the center of the Galaxy than the Sun). The evolution of $M_2(t)/M_2(0)$ for the models is shown in Figure 8.

As was the case for the dwarf galaxies, ionized gas is lost quickly from globular clusters, on time scales $\lesssim 100$ Myr. The critical value $\alpha' \sim 6$ as for the dwarf galaxy. Again, the rapid mass loss induced by tides precludes extended epochs of star formation in these systems. Note that for $\alpha' \sim 1$, the theoretically determined f is much larger than that estimated from (2-12). In this limit, the assumption of quasi-equilibrium breaks down near the Lagrangian point. Nevertheless, the dependence of τ_{loss} on the magnitude of α' is well established.

5. Discussion and Consequences for the Evolution of Dwarf Systems

The essence of our results is contained in Tables 1, 2, and 3. The results of the calculations in §3 indicate that gas in typical dwarf spheroidal galaxies (dSphs) can be fully ionized, even by a modest background UV flux. But for the more extended and dwarf elliptical galaxies, a fraction of the residual gas can remain neutral at their central regions, especially during more recent epochs. Even for these galaxies, mass loss occurs if the dwarf galaxies are captured as satellites of larger galaxies or clusters of galaxies.

As can be seen in the tables, and expected from § 2, the time scale for mass loss is extremely sensitive to the ratio $\alpha \equiv \phi_0/c_s^2$. The magnitude of ϕ_0 can be directly measured from the central velocity dispersion. If $\alpha \gg \alpha_1 \simeq 6 - 10$, then the gas is tightly held within the potential of the dwarf stellar system. The density contrast between the center of the galaxy and the tidal radius, given by Equation (2-7), $\rho(x_t, 0, 0)/\rho(0, 0, 0) \sim \exp(-\alpha) \ll 1$. In this limit, the time scale for mass loss, $\tau_{loss} \gg \tau_d$, where τ_d is the dynamical time scale of the dwarf system. The reverse is true when $\alpha = \phi_0/c_s^2 < \alpha_1$.

For many dwarf galaxies, the velocity dispersion is comparable to the sound speed of ionized gas, and so, if the gas is ionized, the system should have $\alpha \approx 1$. Once $\alpha < \alpha_1$, our results indicate that the gas may be lost to the dwarf system on a time scale no longer than several times τ_d , which is shorter than both the orbital period, P , and the time scale on which subsequent generations of stars would be expected to form (Murray & Lin 1993; Lin & Murray 1994). Multiple possible sources of ionizing radiation exist, including extragalactic UV, UV from a nearby massive galaxy, or UV from stars formed within the dwarf galaxy (Weinberg, Hernquist & Katz 1997; Kepner, Babul, & Spergel 1997; Dong, Murray, & Lin 2003). The evolution of dwarf galaxies therefore depends upon their proximity to a massive galaxy, the source of the ionizing radiation, and when or if the gas within the dwarf galaxies is ionized.

Previous investigation by Kepner et al. (1997) suggest that the external UV radiation in early epochs can fully ionize residual gas in typical-mass dwarf galaxies, and so rapid mass loss might be expected. The results in §3 show, however, that hot ionized gas can be retained in potentials with velocity dispersions comparable to or less than the sound speed of the gas, provided that the host galaxy is isolated. Thus, even in the presence of an intense UV background, low-mass dwarf galaxies do not automatically lose their gas content, albeit the density distribution can become relatively flat for systems which contain hot gas.

Such an environmental dependence may help to explain differences between some types of dwarf galaxies. Dwarf irregular (dIrr) and dwarf elliptical (dE) galaxies are observed to be similar in terms of their dark-matter potentials and ordinary matter content. But, a significant amount of ordinary matter in dIrrs is in the form of gas, whereas little gas is found in dEs. It has been suggested that this difference is due to the efficiency of gas removal (Lin & Faber 1983), motivated by the fact that dEs are primarily located in clusters of galaxies, whereas dIrrs are mostly found in the field. Although the presence of hot gas in clusters of galaxies can lead to efficient stripping (Murray et al. 1993), the present results indicate that tidal effects can also remove the ionized gas in dwarf galaxies within a galactic cluster environment within several Gyr.

At the center of large clusters, however, where the density is nearly homogeneous or declines slowly with radius, the tidal potential is compressive rather than disruptive. In these regions, dwarf galaxies may also be able to retain their gas content, even if it is mostly ionized. Nucleated dwarfs are often found in these central regions of clusters of galaxies. The retention of residual gas may enable the dwarf systems to undergo repeated star formation, possibly leading to the formation of their nucleated structure. This dependence upon location is in the same sense as that proposed by Babul & Rees (1992). In that earlier work, it was proposed that the added confinement by the denser gas near cluster centers would help to prevent supernova-driven mass loss from dwarf galaxies, allowing them to retain their gas for subsequent generations of star formation. Away from the cluster center, however, where tidal forces are disruptive, they shall act in opposition to external confinement, to drive mass loss. In those regions, the presence of a significant external medium may even enhance mass loss, via the Kelvin-Helmholtz instability (Murray et al. 1993).

The evolution of non-isolated dwarf systems depends upon both their masses and their proximity to a massive galaxy. The results in § 4 indicate that if a massive galaxy forms near a dSph prior to the efficient conversion of the internal gas of the dSph into stars, then the remaining gas shall be rapidly lost to tidal stripping if it becomes ionized. In the most extreme case, when background UV heating has ionized the gas within the dSph, preventing it from forming any stars, tidal stripping of the gas shall lead to the formation of a starless, dark-matter mini-halo orbiting the larger galaxy. Only the gas component of the smaller systems is efficiently lost, because the outflow is continually replenished by the attempt to re-establish quasi-hydrostatic equilibrium. The dark-matter mini-haloes may be preserved, because they were formed in relatively high density environments (Moore et al. 1999). Thus, the results presented here naturally imply that the halo of large galaxies may be populated with many ‘stripped’ dark matter, self-gravitating systems.

By contrast, the gas within the most massive dSphs, and that within dEs may be self-shielded, and remain mostly neutral. That, coupled with their deeper potentials, allows them to retain their gas for a much longer time than low mass dSphs, and form multiple generations of stars before losing their gas, even when in close proximity to a massive galaxy. The dependence of the rate of tidal stripping upon the mass of the dwarf system may provide an explanation for the “missing satellite galaxy” problem, because, in accordance with the CDM model, the galactic mass function decreases with M_d .

Tidal loss is also crucial for globular clusters. As in dSphs, $\phi_0^{1/2}$ for globular clusters is a few to a few tens of km s^{-1} , comparable to the sound speed of ionized gas. The highly homogeneous chemical abundance among stars within any given globular cluster (Sandage & Katem 1977; Cohen 1979; Sandage & Katem 1982; Richer & Fahlman 1984; Bolte 1987a,b) requires thorough mixing of the proto-cluster clouds. Even with efficient turbulent mixing, many internal crossing time scales are required (Murray & Lin 1990). Thus, prior to the formation of presently observable stars in globular clusters, gas must be retained for a time comparable to or longer than their Galactic orbital period. The baryonic density of globular clusters is higher than that of dSphs, and so, prior to efficient star formation, the gas was likely to be self-shielded from

external heating. Because the value of α_1 is much larger for cool atomic and molecular gas, the gas can then be retained for several Galactic orbits. Self-gravity of the gas was also probably very important for globular clusters at early epochs, which would further help them to retain their gas.

The internal UV production following efficient star formation within a globular cluster would, however, ionize the gas, after which would be rapidly lost to the system. The same fate would apply to the most massive dSphs orbiting close to a massive galaxy. In the presence of a tidal field, therefore, star formation within dwarf systems can become a self-terminating process, even in the absence of ram pressure stripping, supernova heating, or other means of violent gas ejection.

In the hierarchical galaxy formation scenario, large galaxies are formed through coalescence of dwarf galaxies. Galactic tides enable the rapid decoupling of the gas from dwarf galaxies. The tidally removed gas is detached gently from the dwarf systems, and shall form thin tidal streamers, similar to the Magellanic Stream. These gas streams are dispersed by differential gravity, precession, nonlinear shock dissipation, and drag by the residual gas in the halo. The tidally removed gas does, however, retain its angular momentum. When it is mixed with the residual halo gas, together they can form the disk (Sommer-Larsen, Gelato, & Vedel 1999). The “tidally stripped” dark matter clumps shall themselves undergo subsequent orbital decay due to dynamical friction. In outer regions of the of the large parent galaxies, the residual gas in the halo is tenuous, possibly allowing the streamers to preserve their integrity. Repeated Galactic encounters may lead to recapture of the gas from the streamers by the dwarf system, and induce secondary star formation. The follow-up investigation on the tidally removed gas will be analyzed and presented in subsequent work.

This work was performed under the auspices of the U.S. Department of Energy by University of California, Lawrence Livermore National Laboratory under Contract W-7405-Eng-48. This work is partially supported by NASA through an astrophysical theory grant NAG5-12151.

REFERENCES

- Aaronson, M. 1983, *ApJ*, 266, L11
- Allen, A. J. & Richstone, D. O. 1988, *ApJ*, 325, 583
- Anninos, P., & Fragile, P. C. 2003, *ApJS*, 144, 243
- Anninos, P., Fragile, P. C., & Murray, S. D. 2003, *ApJ*, submitted
- Barkana, R., & Loeb, A. 1999, *ApJ*, 523, 54
- Bechtold, J., Weymann, R. J., Lin, Z., & Malkan, M. A. 1987, *ApJ*, 315, 180
- Benson, A. J., Lacey, C. E., Baugh, C. M., Cole, S., & Frenk, C. S. 2002, *MNRAS*, 333, 156
- Binney, J. & Tremaine, S. 1987, in *Galactic Dynamics* (Princeton: Princeton Univ. Press), 30
- Blumenthal, G. R., Faber, S. M., Primack, J. R., & Rees, M. J. 1984, *Nature*, 311, 517
- Bolte, M. 1987a, *ApJ*, 315, 469
- Bolte, M. 1987b, *ApJ*, 319, 760
- Burkert, A. 1995, *ApJ*, 447, L25
- Cohen, J. G. 1979, *ApJ*, 231, 751
- Cole, S., Aragon-Salamanca, A., Frenk, C. S., Navarro, J. F., & Zepf, S. E. 1994, *MNRAS*, 271, 781
- Dekel, A., & Silk, J. 1986, *ApJ*, 303, 39
- Dong, S., Murray, S. D., & Lin, D., N. C. 2003, *ApJ*, in preparation
- Efstathiou, G. 1992, *MNRAS*, 256, 43P
- Faber, S. M. & Lin, D. N. C. 1983, 266, L17
- Fragile, P. C., Murray, S. D., Anninos, P., & Lin, D. N. C. 2003, *ApJ*, submitted
- Gerola, H., Carnevali, P., & Salpeter, E. E. 1983, *ApJ*, 268, 75L
- Grebel, E. K. 2001, *ASSS*, 277, 231
- Gu, P-G., Lin, D. N. C., & Bodenheimer, P. H. 2002, *ApJ*, submitted
- Haardt, F., & Madau, P. 1996, *ApJ*, 461, 20
- Harbeck, D., Grebel, E. K., Holtzmann, J., Guhathakurta, P., Brandner, W., Geisler, D., Sarajedini, A., Dolphin, A., Hurley-Keller, D., & Mateo, M. 2001, *AJ*, 122, 3092
- Hodge, P. W. 1971, *ARA&A*, 9, 35
- Innanen, K. A. 1979, *AJ*, 84, 960
- Kang, H., Shapiro, P. R., Fall, S. M., & Rees, M. J. 1990, *ApJ*, 363, 488

- Kepner, J. V., Babul, A., & Spergel, D. N. 1997, *ApJ*, 487, 61
- King, I. 1962, *AJ*, 67, 471
- Klypin, A., Nolthenius, R., & Primack, J. 1997, *ApJ*, 474, 533
- Kormendy, J. 1985, *ApJ*, 295, 73
- Klypin, A. A., Kravtsov, A. V., Valenzuela, O. & Prada, F. 1999, *ApJ*, 522, 82
- Lin, D. N. C. & Faber, S. M. 1983, *ApJ*, 266, L21
- Lin, D. N. C., & Murray, S. D. 1992, *ApJ*, 394, 523
- Lin, D. N. C., & Murray, S. D. 1994, in *Dwarf Galaxies (Garching: ESO)*, 535
- Lin, D. N. C., & Murray, S. D. 1998, in *Dwarf Galaxies and Cosmology (Paris: Frontieres)*, 433
- Mac Low, M.-M., & McCray, R. 1988, *ApJ*, 324, 776
- Madau, P., Ferrara, A., & Rees, M. J. 2001, *ApJ*, 555, 92
- Mateo, M. 1996, in *Formation of the Galactic Halo...Inside and Out*, ed. H. Morrison & A. Sarajedini (San Francisco: ASP) 434
- Mateo, M. 1998, *ARA&A*, 36, 435
- Metcalf, R. B. 2002, *ApJ*, 580, 696
- Metcalf, R. B. & Zhao, H. 2002, *ApJ*, 567, L5
- Mori, M., Ferrara, A., & Madau, P. 2002, *ApJ*, 571, 40
- Moore, B., Ghigna, F., Governato, F., Lake, G., Stadel, J. & Tozzi, P. 1999, *ApJ*, 524, L19
- Murray, S. D. & Lin, D. N. C. 1989, *ApJ*, 339, 933 (see also Erratum, 1989, *ApJ*, 344, 1052)
- Murray, S. D. & Lin, D. N. C. 1990, *ApJ*, 357, 105
- Murray, S. D., & Lin, D. N. C. 1993, in *The Globular Cluster–Galaxy Connection*, eds. G. H. Smith & J. P. Brodie (San Francisco: ASP), 738
- Murray, S. D., White, S. D. M., Blondin, J. M., & Lin, D. N. C. 1993, *ApJ*, 407, 588
- Navarro, J. F., Frenk, C. S., & White, S. D. M. 1997, *ApJ*, 490, 493
- Navarro, J. F., & Steinmetz, M. 1997, *ApJ*, 478, 13
- Oh, K. S. & Lin, D. N. C. 1992, *ApJ*, 386, 519
- Ostriker, J. P., & Ikeuchi, S. 1983, *ApJ*, 268, L63
- Plummer, H. C. 1911, *MNRAS*, 71, 460
- Pringle, J. E. 1985, in *Interacting Binary Stars*, ed. J. E. Pringle & R. A. Wade (Cambridge: Cambridge University Press), 1

- Pryor, C. & Meylan, G. 1993, in *Structure and Dynamics of Globular Clusters*, ed. S. G. Djorgovski & G. Meylan (San Francisco: ASP), 357
- Quinn, T., Katz, N., & Efstathiou, G. 1996, *MNRAS*, 278, L49
- Richer, H. B. & Fahlman, G. G. 1984, *ApJ*, 277, 227
- Sandage, A. & Katem, B. 1977, *ApJ*, 215, 62
- 1982, *AJ*, 87, 537
- Sommer-Larsen, J., Gelato, S. & Vedel, H. 1999, *ApJ*, 519, 501
- Tenorio-Tagle, G., Bodenheimer, P., Lin, D. N. C., & Noriega-Crespo, A. 1986, *MNRAS*, 221, 635
- van Zee, L., Skillman, E. D., & Salzer, J. J. 1998, *AJ*, 116, 1186
- Weil, M. L., Eke, V. R. & Efstathiou, G. 1998, *MNRAS*, 300, 773
- Weinberg, D. H., Hernquist, L., & Katz, N. 1997, *ApJ*, 477, 8
- White, S. D. M., & Rees, M. J. 1978, *MNRAS*, 183, 341

Table 1. One-Dimensional Galaxy Models

Model	M_d $10^7 M_\odot$	r_0 kpc	σ km s ⁻¹	α'	J_ν ^a	$\frac{M_{gi}}{M_d}$	$\frac{M_{Hf}}{M_{gi}}$	$\frac{R_E}{R_n}$	P Gyr	τ_{loss} Gyr	$\frac{\tau_{loss}}{P}$	Γ
1D-1	3.66	1	18	0.14	40	0.1	0.15	23.0	3.85	0.7	0.18	0.06
1D-2	3.66	1	18	0.74	1	0.1	0.74	51.0	3.85	6	1.56	0.06
1D-3	3.66	1	18	0.93	0.1	0.1	0.90	8.2	3.85	17	4.42	0.06
1D-4	3.66	1	18	0.41	40	0.2	0.52	39.6	3.85	2.5	0.65	0.06
1D-5	7.32	1.35	21.6	0.18	40	0.1	0.24	183	5.44	2.8	0.51	0.11

^aThe units of J_ν are 10^{-24} erg cm⁻² s⁻¹ sr⁻¹ Hz⁻¹

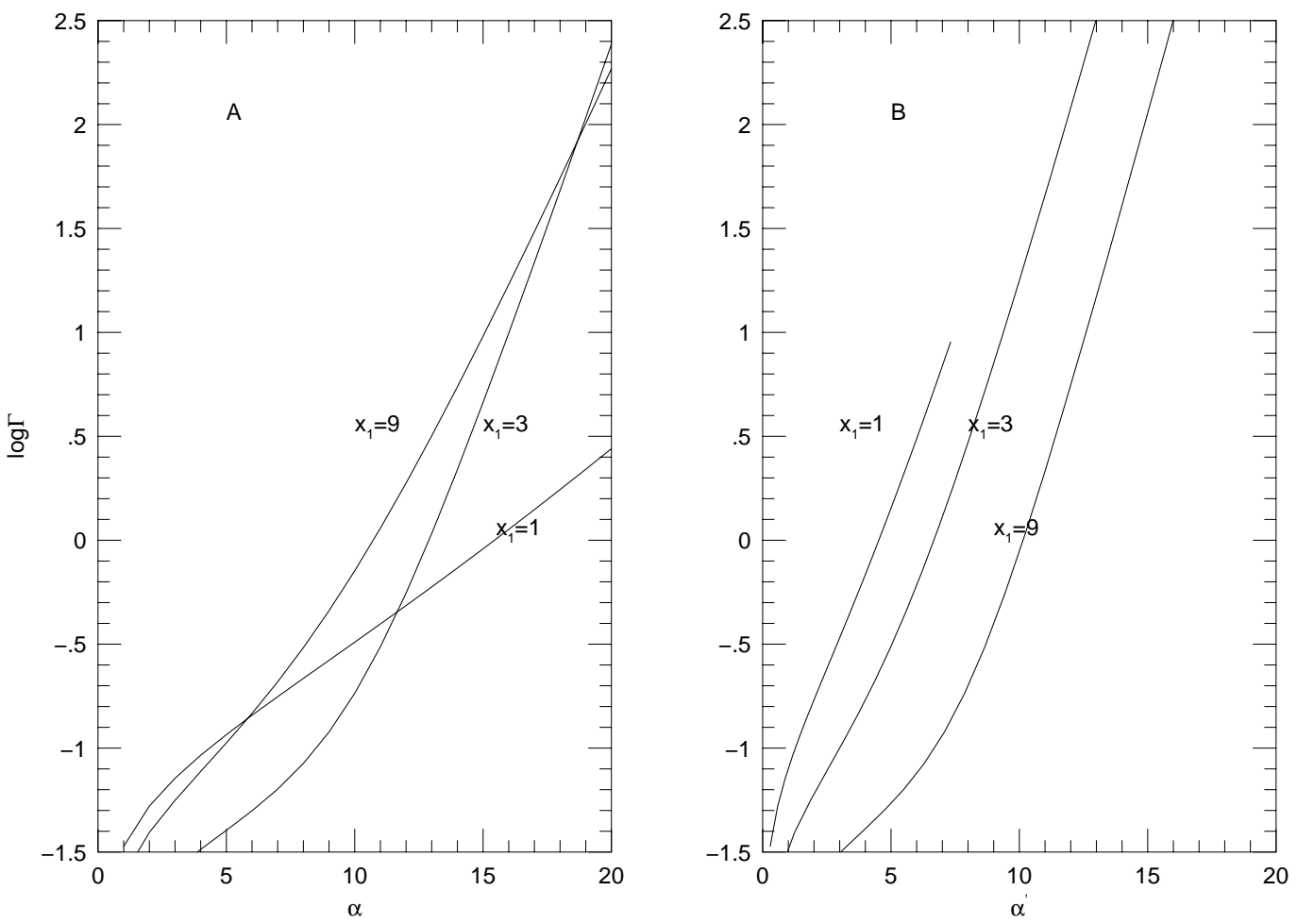
Table 2. Three-Dimensional Galaxy Models

Model units	M_d $10^7 M_\odot$	R_c pc	$\phi_0^{1/2}$ km s^{-1}	a kpc	x_t kpc	T_0 10^3 K	α'	x_R	P (Gyr)	τ_{loss} (Gyr)	Γ	$\frac{P\Gamma}{\tau_{loss}}$	f
3D-1d	1	350	9.2	50	1.1	1	10	3.1	1.4	10	10	1.4	0.17
3D-2d	1	350	9.2	50	1.1	8	1.3	3.1	1.4	0.3	0.04	0.19	1
3D-3d	10	500	26	50	2.3	8	10	4.6	1.4	9.5	2	0.3	0.29
3D-4d	10	500	23	20	1.2	8	8.2	2.5	0.6	1.5	3	1.2	0.16

Table 3. Three-Dimensional Cluster Models

Model	M_{dm} ($10^5 M_\odot$)	R_c (pc)	$\phi_0'^{1/2}$ (km s^{-1})	a (kpc)	x_t (pc)	T_0 (10^3K)	α'	x_R	P (Gyr)	τ_{loss} (Gyr)	$\frac{P\Gamma}{\tau_{loss}}$	f
3D-1g	2	10	9	10	99	1	9.4	9.9	0.29	3.2	0.07	0.77
3D-2g	2	7	11	10	87	8	1.73	14	0.29	0.1	0.06	1
3D-3g	2	7	10	2	34	1	11	4.8	0.06	1.6	0.37	0.27
3D-4g	2	7	10	2	34	8	1.5	4.8	0.06	0.016	0.1	1

Fig. 1.— The dependence of Γ upon α (panel A) and upon α' (panel B) for $x_R = 1, 3, \text{ and } 9$.



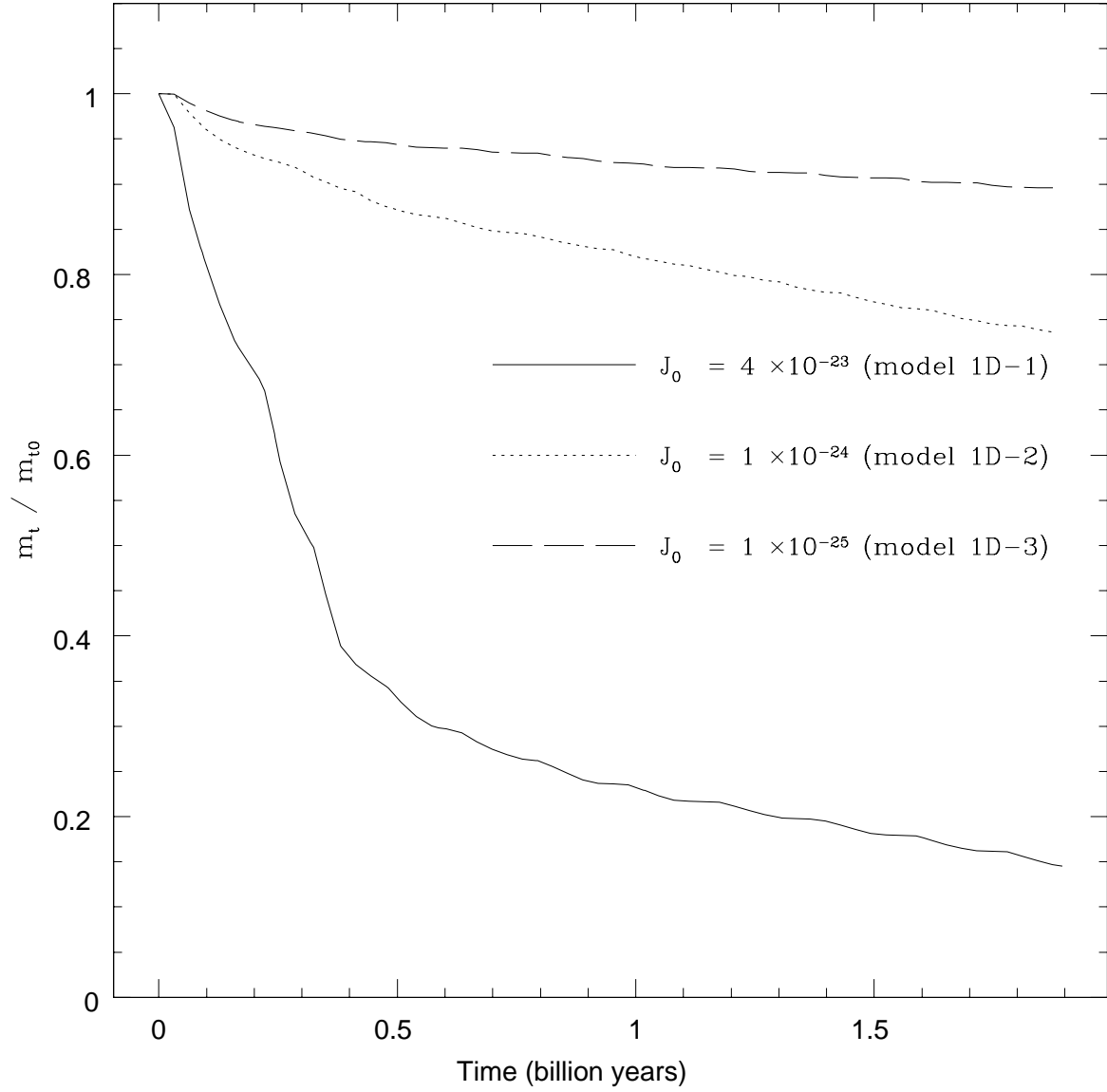


Fig. 2.— Mass of gas contained within the tidal radius as a function of time for the one-dimensional models 1D-1, 1D-2, and 1D-3.

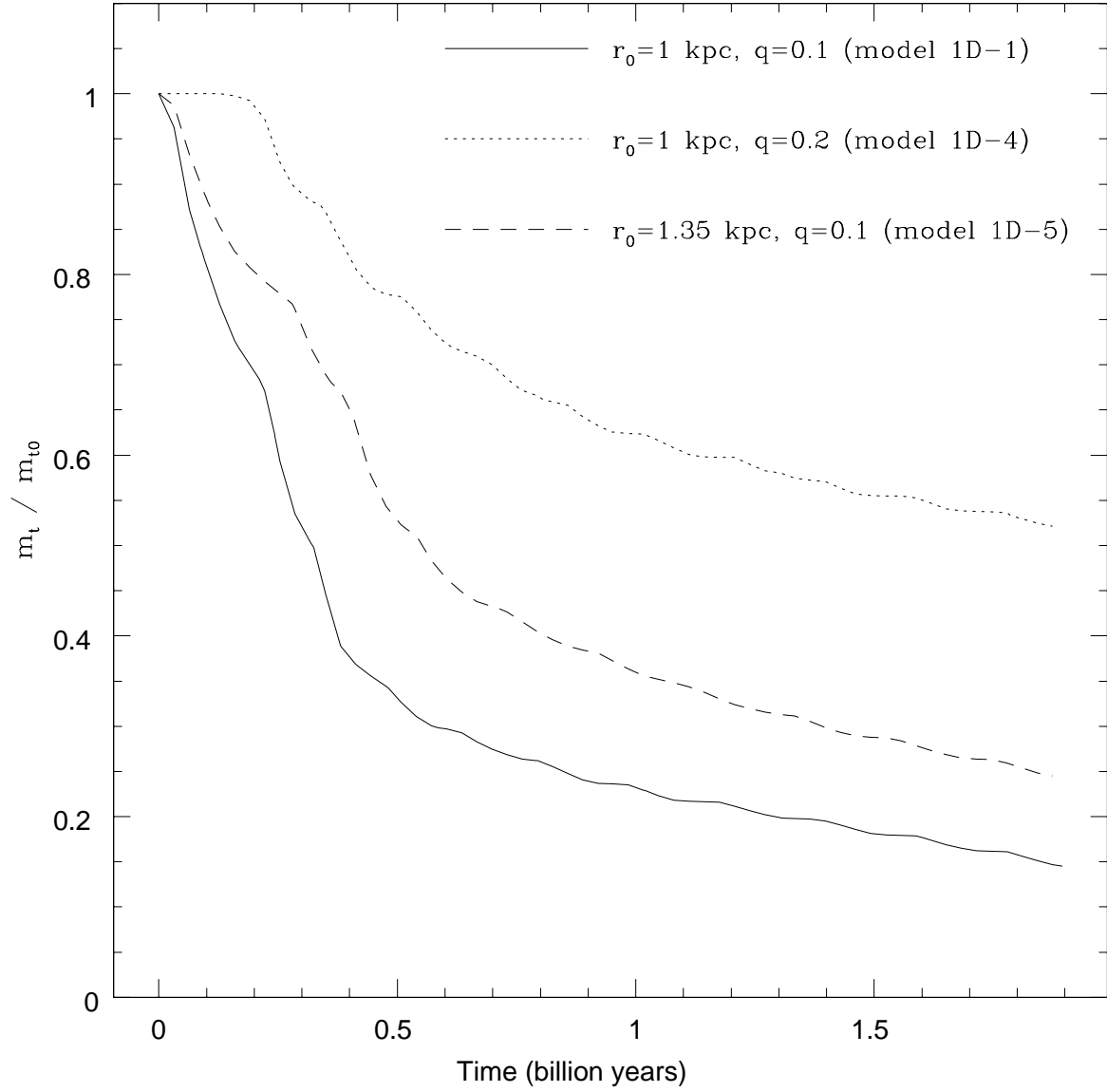


Fig. 3.— Mass of gas contained within the tidal radius as a function of time for the one-dimensional models 1D-1, 1D-4, and 1D-5.

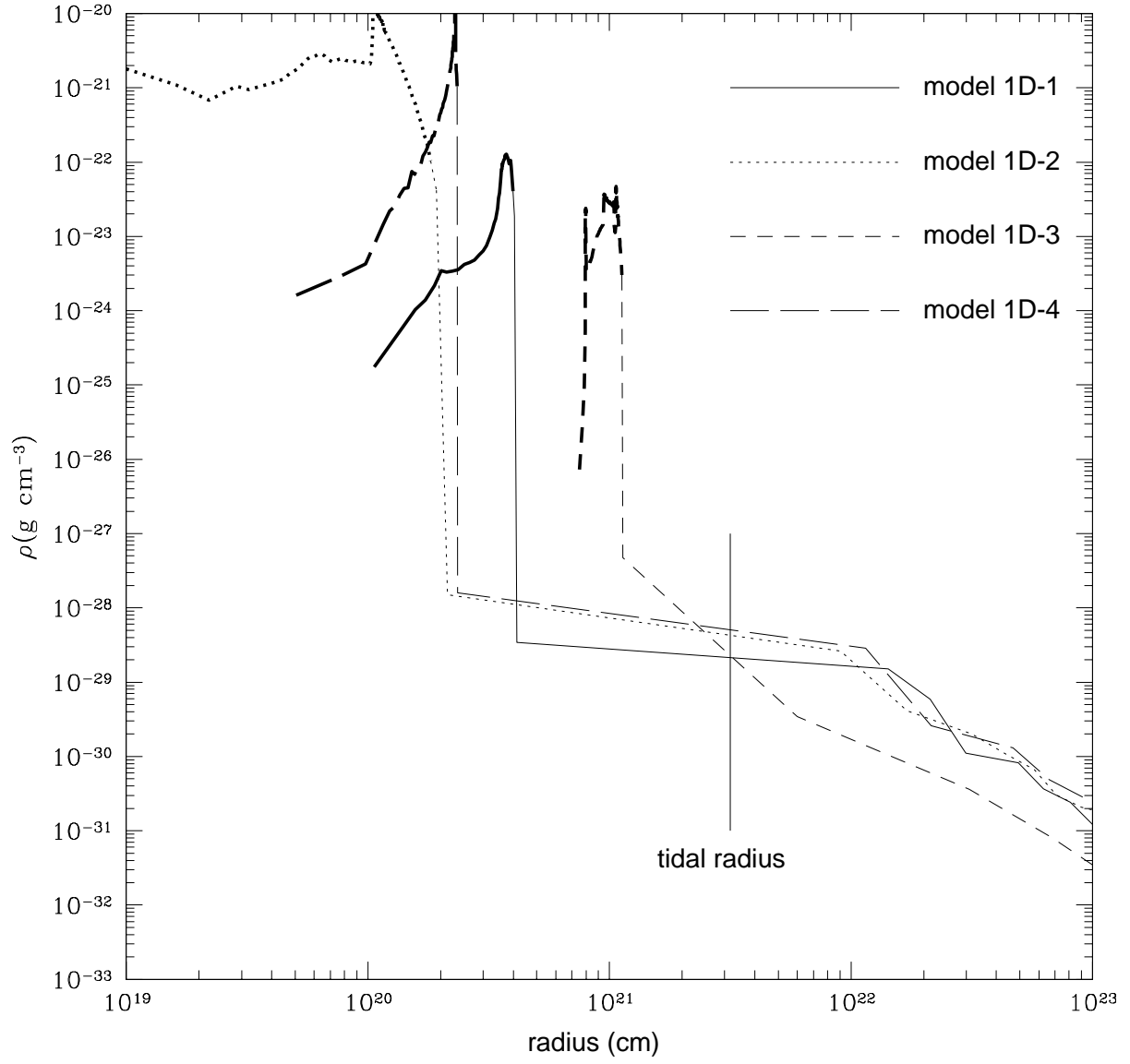


Fig. 4.— Density of gas for the one-dimensional model. The thicker lines denote the density of neutral gas ρ_n , while the thinner ones denote the density of ionized gas ρ_i .

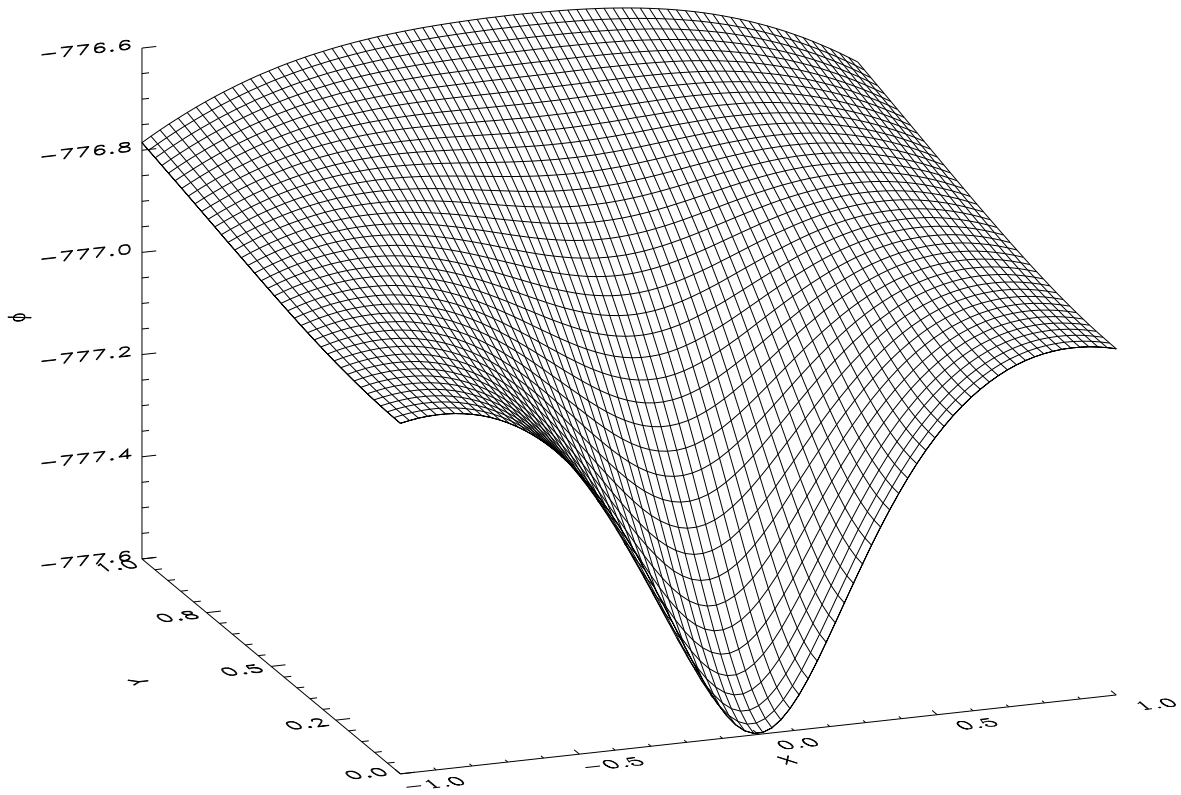


Fig. 5.— Surface plot of $\phi(x, y, z = 0)$ for the three-dimensional galaxy Model 3D-1d. In code units, the y -axis runs from 0 to 1, the x -axis from -1 to 1, and $x_t = 0.89$. The potential, ϕ , is in code units.

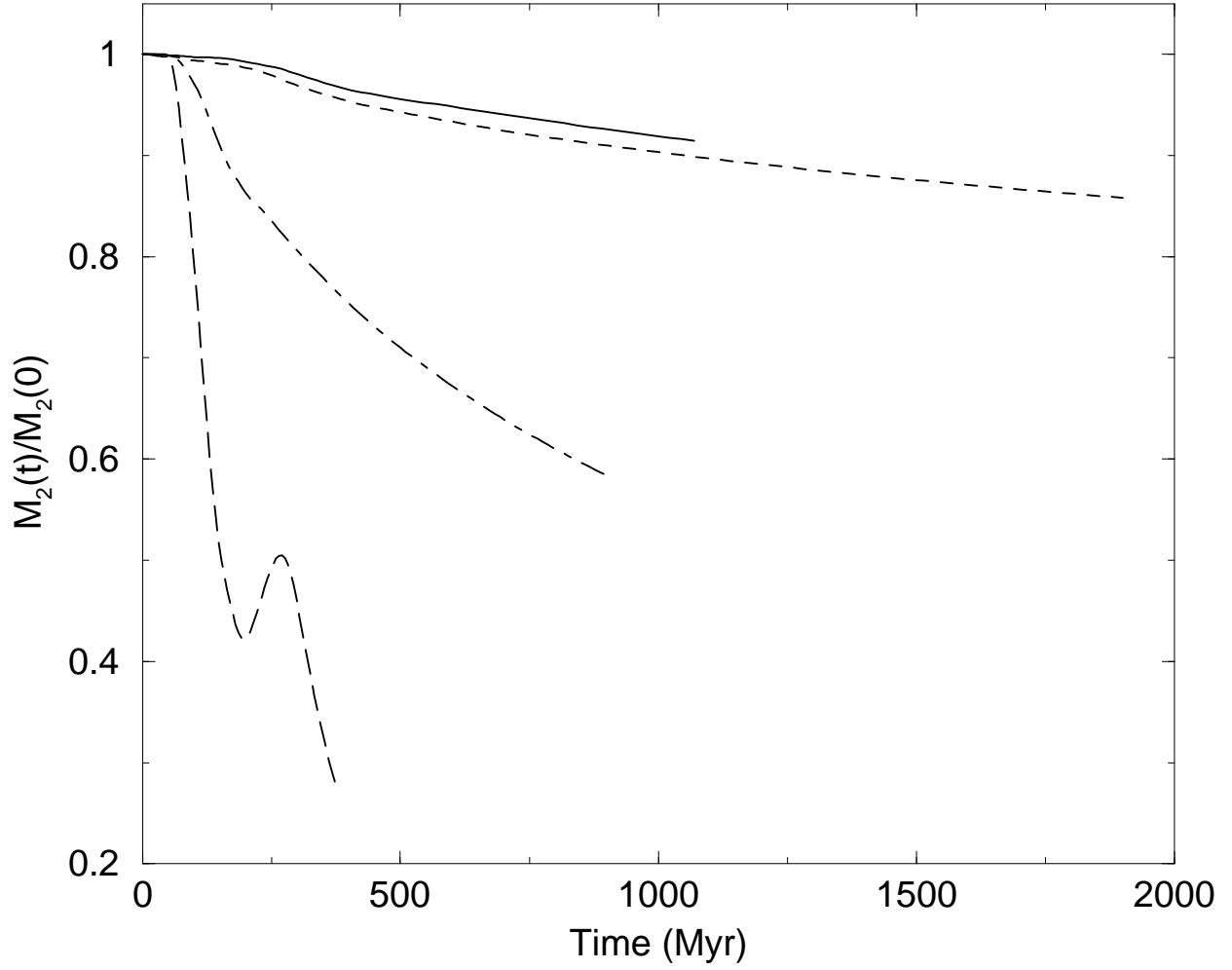


Fig. 6.— The values of $M_2(t)/M_2(0)$ for the three-dimensional dwarf galaxy models. The results for Model 1 are indicated by the solid curve, Model 2 by the long dashed curve, Model 3 by the short dashed curve, and Model 4 by the dot-dashed curve. The values of τ_{loss} are found from exponential fits to the curves.

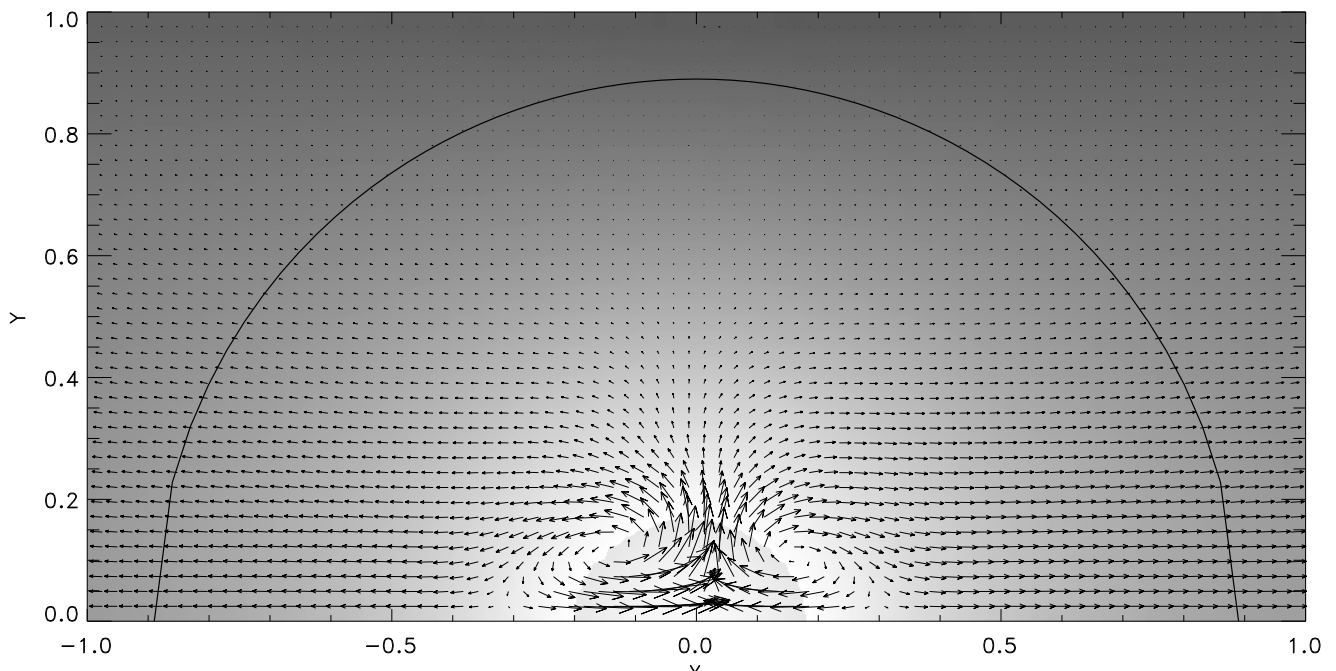


Fig. 7.— The mass flow, $\rho\mathbf{v}$, for the three-dimensional dwarf galaxy model 3D-4d at 680 Myr.

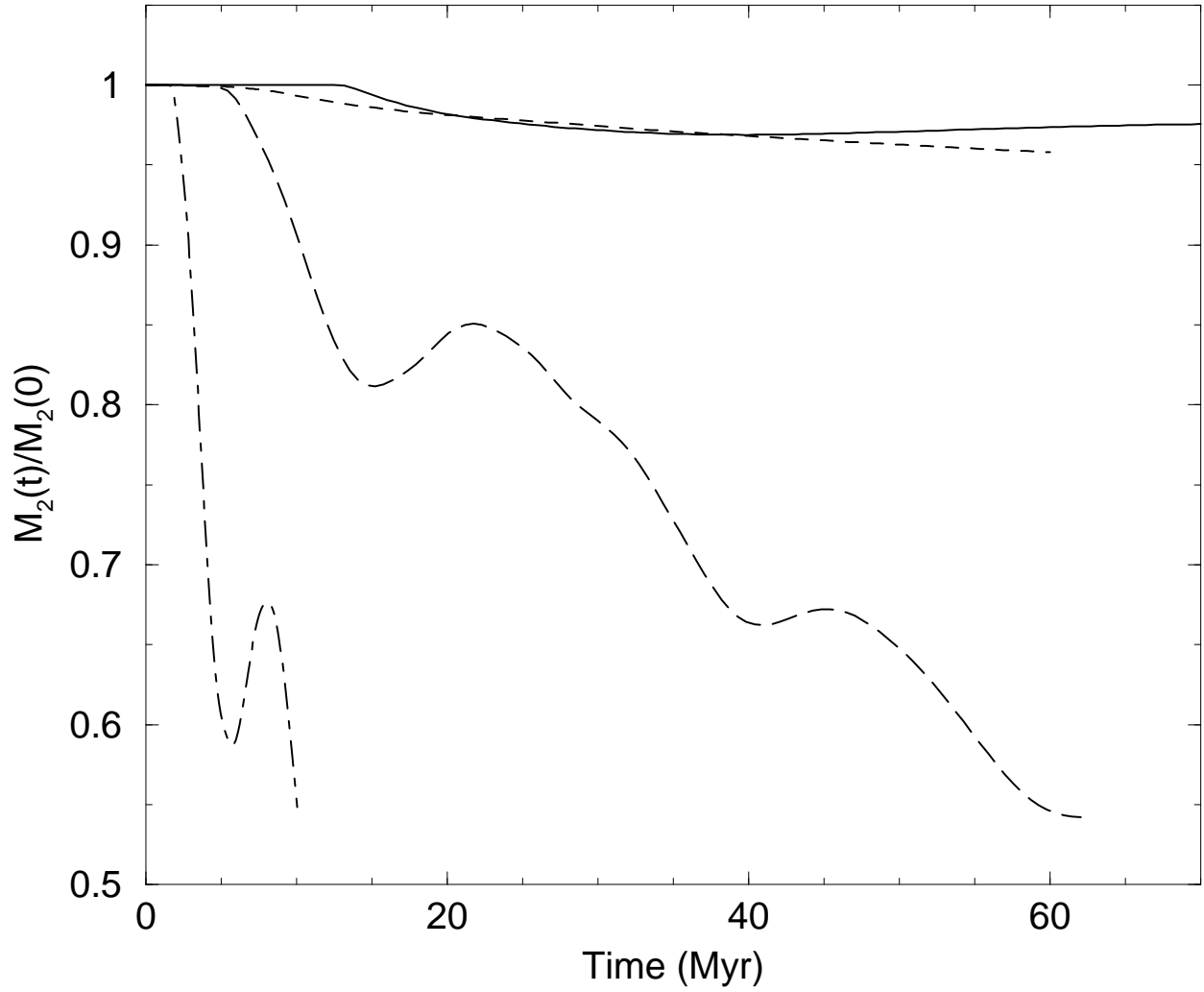


Fig. 8.— The values of $M_2(t)/M_2(0)$ for the cluster models, displayed as in Figure 6.